A98-31502

ICAS-98-2,4,1

NUMERICAL SIMULATION OF THE UNSTEADY AERODYNAMIC RESPONSE OF A COMPLETE AIRCRAFT

H.W.M. Hoeijmakers and S.J. Hulshoff
Department of Mechanical Engineering, Twente University
P.O. Box 217, 7500 AE Enschede, The Netherlands

Abstract

A linearized potential-flow method and an Euler method are applied to the numerical simulation of the unsteady flow aimed at the prediction of longitudinal dynamic parameters for a complete aircraft configuration. Described are the indicial plunge response for a configuration that includes the wing, tail surfaces, the fuselage, the aft-mounted engine nacelle, the engine pylon and the engine exhaust.
The results reveal the importance of considering a detailed model of the complete configuration for the accurate determination of the dynamic response.

Introduction

Present trends towards aircraft designs relying on augmented-stability, and aircraft operating at extreme flight conditions have resulted in a need for an accurate description of the dynamic behavior of aircraft. However, the characteristics of the dynamic behavior can be difficult to obtain during the design phase, due to the necessity of having to predict the steady and unsteady aerodynamic behavior of the complete configuration, this because the dominant effect of the mutual aerodynamic interaction of the various components of the aircraft.
Analytical prediction techniques and empirical methods based on data-bases of the characteristics of existing aircraft are simple to apply, but are limited in their ability to represent the complex aerodynamic interactions occurring in the flow field around realistic configurations. Wind-tunnel tests can be performed, but the requirement for dynamic excitation and measurement significantly increases the complexity and costs of the tests. Therefore, the detailed determination of the dynamic characteristics of the aircraft is often carried out during the flight-test phase, i.e. following the completion of the aircraft design, implying a substantial design uncertainty and risk.
An attractive alternative might be to estimate the aircraft dynamic characteristics using computational fluid dynamics (CFD) methods. CFD techniques can be applied to predict the dynamic characteristics early in the design phase. Furthermore, the CFD methods could be applied to analyze flight conditions which may be difficult or dangerous to reproduce in flight tests.

In general there are two ways to approach the estimation of fluid-structure dynamics using CFD. The first one, known as the coupled-simulation method, integrates the equations for the fluid flow simultaneously with the aircraft kinematic equations. This approach allows all aerodynamic non-linearities to be included in the response of the aircraft. In addition, it is possible to include other features such as control deflections and aero-elastic effects. In spite of its generality, however, at present the coupled-simulation method is too costly to be applied routinely, primarily because of the large number of simulations required to characterize the aircraft response over the full flight envelope. In the second approach, known as mathematical modelling, a range of aerodynamic behavior is encapsulated into compact models of force responses. The parameters in these models can be determined from a relatively small number of CFD simulations for a number of characteristic manoeuvres[1]. In addition to requiring less CFD simulations than for the case of the coupled-simulation approach, the ensuing mathematical models of aerodynamic force responses are efficient to evaluate. This renders them well-suited for implementation in real-time flight simulators and for preliminary flight-control system design.

The range of applicability of a particular CFD technique to the prediction of dynamic characteristics is determined by the approximations inherent in the mathematical model of the fluid flow on which the CFD method is based. At present the most sophisticated model used in aircraft aerodynamics describes the fluid flow by the Reynolds-Averaged Navier-Stokes (RANS) equations. This fluid-flow model allows the representation of effects due compressibility, vorticity, viscosity and heat conduction as well as turbulence (in an approximate fashion through turbulence models) over a wide range of flight conditions.
Flow simulations using RANS methods tend to be costly, however, as high-resolution grids are required to resolve the viscous-flow details. This cost is substantially magnified for unsteady-flow simulations, due to the widely disparate time-scales of high-frequency flow transients and the transients of the aircraft's motion. In addition there is the uncertainty about the applicability of the turbulence model employed in the RANS method.
At the other end of the flow-model spectrum is the linearized potential flow model[2]. Although it can be applied

relatively easily for complex geometries at relatively low cost (both in CPU-time and in man hours required to set up the computational mesh), the linearized potential-flow model cannot represent nonlinear effects (shock waves) due to compressibility nor viscous and heat-conduction effects, nor effects due to turbulence. In addition, the linearized potential-flow model requires the vorticity to be contained within infinitesimal regions, i.e. vortex-wake surfaces and vortex filaments. These vortex sheets have to be fitted into the flow field solution as surfaces across which the velocity potential is discontinuous. Both the strength and the position in space of the vortex sheets have to be determined as part of the solution. Vortex filaments are used as the representation of the compact highly rolled-up parts of the vortex sheets. The topology of the vortex-wake surfaces and vortex filaments is to be specified a priori, which can be a difficult task for complex configurations in unsteady flows.
Practically, however, as computer resources are limited, simplified models of the fluid flow, such as the linearized potential-flow model are required for (design) studies, while more sophisticated models are permissible for occasional insight-providing or validation runs.

A compromise between the two fluid-flow models is the model based on the Euler equations. Typically, aircraft operate in the high-Reynolds-number-flow regime and, at least in part of the flight envelope, at moderate angles of attack, where effects due to viscosity, heat conduction and turbulence are confined to thin shear layers. In these cases the total aerodynamic forces, which are the most significant as far as the dynamic behavior of the aircraft is concerned, can be well predicted by accounting for viscous effects separately. The flow model based on the Euler equations neglects viscosity, heat conduction and turbulence, but retains the ability to accurately represent nonlinear compressibility effects. Furthermore, the Euler equations are able to capture complex wake interactions without the need for an explicit wake model, nor a priori knowledge of wake topology. Although Euler methods do require an order of magnitude larger computational effort than their potential-flow counterparts, Euler methods require considerably less CPU time than RANS methods. Furthermore, numerical techniques generated and experiences gained with Euler methods are also directly applicable to RANS methods, should the latter become more feasible through the rapidly advancing computer technology.

An accurate prediction of the dynamic characteristics of realistic aircraft configurations employing a computational method poses a significant challenge. This is due primarily to the difficulty in predicting the unsteady aerodynamic response, which is often dominated by interactions occurring between time-varying wakes generated by one component interacting with the flow about another component further downstream. These flow interactions have to be resolved adequately, both spatially and temporally. A notable example is the lag in the response of an aft-mounted tail, a lag caused by the finite time it takes for the wing wake vorticity to get convected to the tail of the configuration. Such an interaction can have a strong influence on the aerodynamic damping of short-period dynamic modes. Therefore, a numerical method used in the prediction of dynamic responses must be sufficiently general to represent the complex geometry of the aircraft configuration as well as the complex flow features and interactions occurring during the response. However, the method must also be computationally efficient, so that it can be applied to numerical simulations involving a large number (for an Euler method: order of magnitude 1 to 2 million for the half-space) of grid points, specifically in the vortical wakes.

This paper discusses the development and application of two computational methods for the computation of the aerodynamic responses of manoeuvring complete aircraft configurations. The first of these is based on a surface singularity technique for the linearized potential-flow equation. This (panel) method allows the consideration of complex geometries at minimum cost, making it suitable for design purposes. The second computational method is based on a solution algorithm for the Euler equations. This algorithm is suitable for the numerical simulation of the aerodynamic response at conditions with complex vortical-wake interactions and cases with significant compressibility effects. The algorithm has been implemented with an emphasis on ensuring efficiency, both in terms of accuracy for a given number of grid points, and work per grid point per time step, but does require significantly more computational effort than the panel method. Although a conventional structured patched multi-block finite-volume approach is employed, an unstructured patched-interface capability has been included to provide greater control over local grid discretizations and to ease the construction of the multi-block spatial grid. To allow for the large time steps appropriate for low-frequency aircraft manoeuvres, an implicit time-integration procedure is used. This has been implemented using a multi-block sub-iteration technique.

In this paper we present results for the application of the potential-flow method and the Euler method to the prediction of indicial-plunge aerodynamic responses.

Aerodynamic Responses

In flight dynamics, the aerodynamic characteristics of aircraft are normally expressed in terms of aerodynamic stability derivatives, which are the parameters of the mathematical models of the aerodynamic response. The majority of these parameters are associated with a steady flight condition. Therefore these stability derivatives can be ex-

tracted from the steady-flow solution of the computational method, i.e. the panel method or the Euler method. For the steady stability derivatives it is assumed that the total aerodynamic force (and moment) is a function of the instantaneous state variables only. The history of the manoeuvre is thus neglected. During the rapid actuation of the controls, however, unsteady interactions between aircraft components, such as the wing and the tail, can have a significant effect on the dynamic response. For longitudinal motions, this is often accounted for with additional derivatives associated with the instantaneous time-derivative of the angle of attack ($\dot{\alpha}$). Estimation of these derivatives requires computationally intensive, time-accurate, simulations of the flow around the aircraft.

An often employed strategy is to evaluate the $\dot{\alpha}$-derivatives using the force response from harmonic α excitations. Since the $\dot{\alpha}$-derivatives depend on the frequency a number of flow simulations are required to establish the frequency response. To obtain the harmonic response, however, requires long time-histories of the response before the initial transients have damped out. Therefore this strategy requires excessive computer resources.
A possibly more efficient strategy for determining the unsteady aerodynamic response is by the computation of indicial functions, which are the responses to step inputs of for instance angle of attack. Employing the indicial-function approach the frequency-response to unsteady excitations about a mean state can be determined using the results of just one, relatively short-duration, time-accurate flow simulation. Indicial responses can also be used to construct more general models of aerodynamic force response, which can include aerodynamic hysteresis and bifurcations [3]. The results of the indicial response computation can be related to the unsteady stability derivatives, such as the $\dot{\alpha}$-derivatives, through for example the method described in Refs. 3 and 4.

The time-variant lift response to a time-dependent α, $C_L(t)$, can be expressed in terms of the indicial response $A(t)$ to a unit change in α as:

$$C_L(t) = C_L(0) + \int_0^t A(t-\tau)\frac{d\alpha(\tau)}{d\tau}d\tau \qquad (1)$$

Assuming that $\dot{\alpha} = d\alpha/dt$ is constant we get:

$$C_L(t) = C_L(0) + \dot{\alpha}\int_0^t A(t-\tau)d\tau \qquad (2)$$

Noting that the final response to a unit change in α is $C_{L\alpha}$, and defining a lift-defect function as $f(t) = C_{L\alpha} - A(t)$, the lift response follows as:

$$C_L(t) = C_L(0) + C_{L\alpha}\dot{\alpha}t - \dot{\alpha}\int_0^t f(t-\tau)d\tau \qquad (3)$$

Since $\dot{\alpha}t = \alpha(t)$, Eq. (3) can be expressed in terms of standard stability derivatives if we define:

$$C_{L\dot{\alpha}} = -\int_0^t f(t-\tau)d\tau \qquad (4)$$

The determination of indicial responses for airfoils and finite-span wings has been considered theoretically by amongst others Bisplinghoff et al.[5], experimentally by amongst others Leishman[6] and more recently numerically by amongst others Lesieutre et al.[7]. In two dimensions theoretical results include both results for incompressible flow as well as approximate results for compressible flow. In three dimensions analytical results for incompressible flow include approximate results for thin wings of elliptical, rectangular and delta planform of various aspect ratios.

The indicial response of the aerodynamic force and moment may be split into a circulatory and a non-circulatory part. The circulatory part contains the persistent influence of the generation of vorticity at the trailing edges of the configuration as a response to the excitation of the state of the aircraft. The non-circulatory part is due to the acoustic wave system created by the initial step change in the state of the aircraft. In incompressible flow the acoustic speed is infinite and the non-circulatory part reduces to an infinite pulse occurring at the initiation of the excitation. In compressible flow the initial non-circulatory part is finite, and its influence persists for the early portion of the response history. For example for a wing responding to a sudden increase in angle of attack, this initial loading is caused by the creation of uniform compression and expansion waves on the upper and lower surface, respectively. As shown by Lomax[8] the magnitude of the initial response can be determined in a manner similar to that for a one-dimensional piston. As time proceeds, acoustic waves propagating from the edges of the wing destroy the initially uniform distribution of the pressure perturbations. The reflections and interactions of these waves determine the later form of the non-circulatory response, see Lomax[8].
In both incompressible and compressible flow, the later portions of the indicial response are dominated by the circulatory effects, i.e. convection of vorticity generated at the edges and interaction of this vorticity with the flow around the generating component as well as around downstream aircraft components. In the case of an isolated finite-span wing, vorticity generated at the wing's trailing edge has a time-variant influence on the wing surface pressure distribution as the vorticity is convected in downstream direction, away from the wing trailing edge. An isolated wing therefore approaches its final loading asymptotically. In case more than one aircraft component is present, however, the influence of the wake vorticity convecting downstream from one component may induce a significant perturbation to the response of another compo-

nent. Conversely, the flow field and wake geometry may also be distorted by the unsteady loading (bounded vorticity) of the affected components, possibly leading to a significant unsteady aerodynamic coupling.

Potential-flow method

Assuming that for the high-Reynolds-number flow the influence of viscosity, heat conduction and turbulence is limited to thin layers and can be neglected, and assuming that the vorticity is contained within infinitesimal regions such as vortex sheets and vortex filaments a velocity potential can be introduced as $\vec{u}(\vec{x},t) = \vec{\nabla}\Phi(\vec{x},t)$, with $\Phi(\vec{x},t)$ the velocity potential. In the present paper we consider incompressible potential flow only. In that case (see Ref. 2) the governing equation for the velocity potential is Laplace's equation:

$$\frac{\partial^2\Phi}{\partial x^2} + \frac{\partial^2\Phi}{\partial y^2} + \frac{\partial^2\Phi}{\partial z^2} = 0 \qquad (5)$$

Once the velocity potential has been obtained, the pressure follows from Bernoulli's equation:

$$\frac{\partial\Phi}{\partial t} + \tfrac{1}{2}|\vec{\nabla}\Phi|^2 + \frac{p}{\rho} = C(t) \qquad (6)$$

with C(t) an arbitrary constant, here related to the flow at infinity upstream.
The solution of Laplace's equation, Eq. (5) is expressed in terms of doublet distribution μ and source distribution σ on the surface of the geometry and a doublet distribution on the wake vortex sheets trailing from the trailing edges of the lifting components of the aircraft. Both singularity distributions are a function of location on the surface as well as of time.

The boundary conditions to be imposed are the following:

(1) On solid surfaces, which are assumed to be closed, i.e. bound a volume, the normal-velocity boundary condition is imposed through a Dirichlet condition for the fictitious flow (which can be chosen conveniently) inside the volume enclosed by the surface. This leads to an algebraic relation for the strength of the source distribution and a Fredholm integral equation of the second kind for the doublet distribution.

(2) On wake vortex sheets three conditions apply, namely that it is a stream surface and that the static pressure is continuous across the vortex sheet. This gives, at least in principle, sufficient conditions for determining the unknown position of, and the unknown doublet distribution on, the wake vortex sheet. The shape of the vortex sheet varies in time and can become quite complex. For cases of not too high loading and not too large distortions we describe the wake vortex sheet as a distortion superposed on a fixed reference wake surface, i.e. points on the wake vortex sheet are described as:

$$\vec{x}(s_1,s_2,t) = \vec{x}_w(s_1,s_2) + \epsilon(s_1,s_2,t)\,\vec{n}_w(s_1,s_2) \qquad (6)$$

where $\vec{x}_w(s_1,s_2)$ describes the reference wake surface in terms of surface coordinates s_1 and s_2, $\vec{n}_w(s_1,s_2)$ is the unit normal on the wake reference surface and $\epsilon(s_1,s_2,t)$ is the time-dependent distortion, assumed to be small. Exploiting the order of magnitudes of the various quantities involved in a fashion similar to lifting-surface theory, the wake boundary conditions can be linearized to the following two conditions, to be imposed at each point (s_1,s_2) on the wake reference surface at each point in time, see Weber[9]:

$$\begin{aligned}\frac{\partial\mu}{\partial t} &= \vec{u}^P(\vec{x}_w(s_1,s_2),t)\cdot\vec{\nabla}\mu(s_1,s_2,t) + \text{h.o.t.}\\ \frac{\partial\epsilon}{\partial t} &= \vec{u}^P(\vec{x}_w(s_1,s_2),t)\cdot(\vec{n}_w(s_1,s_2) - \vec{\nabla}\epsilon(s_1,s_2,t)) + \text{h.o.t.}\end{aligned} \qquad (7)$$

where $\vec{u}^P(\vec{x}_w(s_1,s_2),t)$ denotes the Principal Value of the sum of the free-stream velocity and the velocity induced by the surface singularity distributions. The upper relation in Eq. (7) is the linearized pressure condition, which does not involve the distortion $\epsilon(s_{1,2},t)$ of the wake vortex sheet, only the known wake reference surface, the unknown doublet distribution on the wake reference surface and the unknown singularity distributions on the solid surfaces enter in this relation. This implies that the wake surface distortion, to first-order approximation in terms of perturbations to the steady-flow solution, does not affect the wake doublet distribution. Once at a given point in time the doublet distribution has been solved for, the wake distortion $\epsilon(s_{1,2},t)$ can be obtained from the lower relation in Eq. (7). This decoupling facilitates the full utilisation of the steady-flow method in a quasi-steady fashion, but for the inclusion of the time-derivative in the upper relation of Eq. (7). Note that this relation is only mildly non-linear in the unknown doublet distribution.

The second-order accurate discretisation of the computational method (FASDU) is described in Ref. 9. It follows the lines sketched in Ref. 2 and involves the subdivision of the surface into mutually independent segments (networks), each divided into panels by s_i = constant and s_2 = constant curves. A local, quadratic, representation is used to describe the geometry of the panels on the solid and on the wake reference surface. The doublet distribution on each panel of these surfaces is approximated using the same type of local, quadratic, representation in terms of s_i and s_2. The source distribution on the solid surfaces is approximated, consistently, employing a linear local representation. Applying the boundary condition(s) at the midpoint of each panel on the solid (and wake reference) surface yields a system of algebraic equations, where most equations are linear in terms of the parameters that define the local quadratic representation of the doublet distribution, while the equations corresponding with the boundary condition on the wake reference surface is qua-

dratic in these parameters. This system is solved using a Newton-Raphson iterative method.
The method only requires the discretisation of the surface of the configuration (dimension-lowering property of the surface-singularity solution technique of solving Laplace's equation), but the calculation of the fully-populated matrix with Aerodynamic Influence Coefficients (AIC's) requires an effort that scales quadratically with N_{panel}.
The potential flow formulation can be extended to the case of compressible flow, resulting, upon linearisation, in the Prandtl-Glauert equation, which now does contain time-derivatives. This implies that in compressible flow the time lag is to be included in the formulation, which is a significant complication.
More details on the method as well as applications to harmonically oscillating airfoils, finite-span wings and wing-tail combinations can be found in Ref. 9.

Euler method

If all quantities are measured relative to the inertial frame, the Euler equations for an arbitrary, moving, control volume V(t) can be written as, see for example Ref. 10:

$$\frac{d}{dt}\int\int\int_V U\,dV + \int\int_{\partial V} \vec{F}(U).\vec{n}\,dS = 0 \qquad (8)$$

where ∂V is the closed surface bounding the control volume V, with $\vec{n}$ is the outward unit normal vector, pointing out of V. The column vector U of the conservation variables is given by $(\rho,\rho u,\rho v,\rho w,\rho E)^T$, where $\rho(\vec{x},t)$ is the density, $\vec{u}(\vec{x},t) = (u,v,w)^T$ the velocity vector and E the total energy per unit mass, which for a calorically perfect gas can be expressed as:

$$E = \frac{1}{\gamma-1}\frac{p}{\rho} + \tfrac{1}{2}|\vec{u}|^2 \qquad (9)$$

with p the static pressure. If we define the velocity of the bounding surface of the control volume as $\vec{u}_{\partial V}$, the normal component of the flux can be expressed as:

$$\vec{F}.\vec{n} = \begin{pmatrix} \rho(\vec{u}-\vec{u}_{\partial V}).\vec{n} \\ \rho\vec{u}(\vec{u}-\vec{u}_{\partial V}).\vec{n} + p\vec{n} \\ \rho E(\vec{u}-\vec{u}_{\partial V}).\vec{n} + p\vec{u}.\vec{n} \end{pmatrix} \qquad (10)$$

In order to discretize the Euler equations the space around the configuration is first divided into blocks, which in turn are divided in structured meshes of hexahedral cells. Eq. (8) is then applied to each cell of the grid, employing a cell-centered finite-volume discretization, resulting in the following system of ordinary differential equations to be integrated in time:

$$\frac{d}{dt}(UV_{cell}) = -\sum_{m=1}^{M_{cell}} \vec{F}_m.\vec{S}_m \qquad (11)$$

where m is the cell-face number, M_{cell} is the total number of faces of the cell surface, V_{cell} is the cell volume and $\vec{S}_m$ is the area vector of cell-face m (unit outward vector times area of cell face).
In the current algorithm the cell-face flux vector may be determined by an upwind scheme, using Roe's approximate Riemann solver with second-order TVD limiting (see Refs. 10 and 11), or by a centered method with scalar nonlinear artificial dissipation.

The time-accurate solution of the Euler equations requires the integration of the system of nonlinear ODE's given in Eq. (11), which can be expressed as:

$$\frac{dU}{dt} = -R(U) \qquad (12)$$

For unsteady flows the choice between explicit and implicit time integration is determined by:
(1) the maximum allowable time step of the explicit scheme relative to the time scale of the problem, and
(2) the work per time step required by the implicit scheme relative to that of the explicit scheme.

In the case of aircraft dynamics the physical time scales are typically several orders of magnitude greater than those allowed for an explicit scheme on a sufficiently refined grid. Thus implicit time integration is to be preferred. In the present method an implicit, multi-grid time-integration has been adopted.
Following Jameson[12], Eq. (12) is reformulated as:

$$\frac{dU}{d\tau} = \frac{dU}{dt} + R(U) = -R^*(U) \qquad (13)$$

where τ can be regarded as an additional independent coordinate. Once we have obtained the solution that is "steady" in τ, we have progressed the solution to the next point in real time. Eq. (13) is discretized by applying a second-order backward scheme to the derivative with respect to t, which in case of constant time step Δt, yields the following implicit scheme for U at time level n+1:

$$\frac{dU^{n+1}}{d\tau} = \frac{3U^{n+1}-4U^n+U^{n-1}}{2\Delta t} + R(U^{n+1}) = -R^*(U^{n+1},U^n,U^{n-1}) \qquad (14)$$

where n is the time-step number. U^{n+1} can then be found by computing the steady solution in τ. This implicit formulation for U^{n+1} removes the theoretical stability restriction, and thus allows the time step Δt to be chosen as the minimum required to accurately resolve the physical process.
The sub-iteration procedure in τ does not need to be implicit, nor accurate. This allows the use of a wide range of acceleration techniques. The present method uses a 5-stage Runge-Kutta integration routine, optionally augmented by local time-stepping (in τ) and residual smoothing. A three-level V-cycle multi-grid procedure is used to accelerate the sub-iteration process.

Although structured multi-block grids can be efficient in terms of memory usage and vectorisation, it can be difficult to generate a high-quality grid about a complex aircraft configuration. For configurations involving multiple components the structured grid approach leads to a large number of blocks, with levels of discretisation which may be inappropriate for local flow details, or may hamper the convergence of the sub-iteration process. One method of reducing the number of blocks, and therewith decreasing the number of continuous-flow block interfaces, increasing the number of cells per block, which is positive for vectorisation, is allowing per cell face more than one boundary condition. A further improvement is to allow changes in grid resolution across block interfaces. However, care must be exercised to maintain the conservation properties of the original algorithm.

In the present method the block interfaces with differing discretisations are treated using an unstructured patched grid approach. Similar to the method of Klopfer et al.[13], the new interface is not defined by one of the two block faces, but instead by the union of the sets of points defining each of the two interfaces. An unstructured lattice of triangular cell faces is then constructed to allow the transfer of fluxes across the interface. This implies that the cell face bordering the interface becomes multi-faceted, and the edges of the cell face on the interface becomes modified. To maintain conservation the surface area vectors of the cell faces on the interface must be corrected to account for the presence of the interface. In order to maintain time-accuracy it is also necessary to correct the cell volume. More details on the treatment of the patched block interfaces is given in Ref. 14.

Refs. 15-17 provide a number of applications of the present method.

Computed Results

To demonstrate the capability of the methods results are presented for a number of configurations, namely an isolated finite-span wing, a wing-tail configuration, and finally a complete configuration.

Isolated Rectangular Wing

The test case chosen is the rectangular wing of aspect ratio 6. The wing has either a constant NACA006 or a constant NACA0012 airfoil section. The panel method used 48 chordwise panels in a so-called double-cosine distribution (refinement near the leading edge and on the upper and lower surface near the trailing edge), and 20 spanwise strips in a half-cosine distribution (refinement near the wing tip. As wake reference surface served the horizontal plane emanating from the wing's trailing edge and extending to infinity downstream, with a half-cosine distribution (refinement near the wing trailing edge) of 18 streamwise panels, closed off with a panel of semi-infinite extent.

Fig. 1 compares analytical results with numerical results for the indicial plunge response of the wing. The quantity k1(s) is the instantaneous lift coefficient divided through the steady-flow lift coefficient as a function of the number of half-chords travelled since the step change in the state (time corresponds to s/U_∞).

The numerical results obtained with the panel method are compared with analytical results calculated by W.P. Jones[18] for a zero-thickness wing, as described in Ref. 19. In a fashion similar to the non-circulatory component of the analytical response (a delta function) the numerical results include a pulse-like behavior at the initiation of the indicial plunge. In the numerical case this is the result of the large change in the surface velocity potential caused by the discontinuous change in the normal-velocity boundary condition between the initial and plunging states.

Beyond time zero, the computed results for both the 6% and the 12% thick wings agree qualitatively with the analytical result, with the 6%-thick wing providing the better agreement with the analytical result for the zero-thickness wing. Clearly as time progresses and the vorticity generated at the trailing edge at time zero is convected more and more aft the lift coefficient tends to its steady-state value in a monotonic manner.

Ref. 9 contains similar comparisons as shown here for the case of a harmonic pitch excitation, showing good agreement between Jones's[18] results and the results of the unsteady potential-flow method.

Fig. 2 shows fine- and coarse-grid results obtained with the present Euler method for the AR = 6 wing at a Mach number of 0.3. The grid is CO-topology grid with 250,000 cells on the fine grid. The 31,250-point coarse grid is obtained from the fine grid by omitting alternate grid points.

In Fig. 2 the lift coefficient is shown as a function of the number of half-chords travelled per radian angle of attack change. Both results contain short-duration oscillations in the very early portions of the response. Although the amplitude and the form of the oscillations are similar those observed in the fine-grid result occur in about half the time of those in the coarse-grid result, this for (physical) time steps of comparable magnitude. The oscillations appear to be represent the limit for each grid for the representation of high-frequency components of the response. This consequence of imposing an infinite acceleration on a geometry with finite discretization is discussed by Lesieutre et al.[7], who suggest a remedy to eliminate the oscillations by using a ramped change of angle of attack, which follows from Laplace-domain inference of the indicial response. However, the results for the two-dimensional flow cases considered in Ref. 7 contain more severe oscillations, possibly due to a lack of the 2D/3D relief effect. The good agreement of the present results for the fine and the coarse mesh, after the initial oscillations, indicates that the discretization errors which are introduced are limited to the very initial phase of the response.

Fig. 2 illustrates that for compressible flow the pulse has a finite duration of about the time needed to travel half a chord. Following this period the wing lift coefficient increases monotonically to its steady-flow value, clearly no aerodynamic interaction can occur in this isolated-wing case.

Fig. 3 compares the potential-flow C_L per radian with the result obtained on the fine grid with the Euler method for a free stream Mach number of 0.3, also included in Fig. 2, and the result for $M_\infty = 0.5$. Clearly, the non-circulatory part of the response affects a significant portion of the response, a portion that increases as the Mach number increases. The extent of the influence of the non-circulatory part is determined by the propagation and interaction of waves emanating from the edges of the wing, destroying the initially uniform pressure perturbation on the wing's upper and lower surfaces. The rate of propagation of these waves is directly related to the speed of sound (see Lomax[8] and Singh et al. [20]), so that at a high Mach number at a fixed speed of sound, the wing will travel more half-chords before a wave emanating from the wing tip, for example, can reach the wing root.
In contrast to the region where the non-circulatory part dominates the response, in the remainder of the region where the circulatory part is the only part left, the influence of the Mach number on the asymptotic rate at which the steady-flow C_L is reached, is small. In fact, the circulatory regions can be made to collapse on a single curve using a compressibility correction appropriate for steady flows, such as the Prandtl-Glauert correction.

Wing-Tail Configuration

Before proceeding to the response of the complete aircraft configuration, it is useful to consider simpler geometric model. Here we choose the wing and the tail of the complete configuration to be considered, the Cessna Citation II. For this aircraft both the wing and the tail have tapered planforms and the tail is positioned about 3 wing root chords behind the wing trailing edge and about 1 root chord above the wing. Indicial response computations using both the panel method (for incompressible flow) and the Euler method were performed for a zero initial α, with a stepwise change in α of 2.4 deg. The potential-flow computations were performed using a 1300 panel half-domain surface discretization, shown in Fig. 4. The reference wake surfaces of both lifting components consist of planes emanating from the trailing edge and trailing straight back. Unlike in the case of the isolated finite-span wing, now the discretization of the wing wake reference surface must be kept relatively fine between the wing's trailing edge and the tail, this in order to properly represent its time-variant influence on the flow around the tail through the vorticity convecting along it in downstream direction. In this case the position and shape of the wake reference surface is now also more important than in the isolated wing case. Low-aspect-ratio wings at higher lift coefficients, for example, would require a more accurate representation of the vortex-wake roll-up than presently used (none). However, for the high-aspect-ratio wing and low lift coefficients considered, a planar wake reference surface can be expected to be adequate. This was confirmed by the shape of the near-wake observed in the solution produced by the Euler method. In the present paper indicial responses are discussed, Ref. 9 presents results for a harmonic response.

The Euler method was applied at a Mach number of 0.5, using a CH-grid, see Fig. 5, with 1.1 million grid points in the half-space. A relatively fine discretization was used in the region between the wing trailing edge and the tail in order to limit the numerical dissipation of the wing wake and to improve the accuracy of the prediction of its influence on the tail. Ref. 15 describes results obtained with this grid topology for varying levels of refinement.

The importance of aerodynamic interactions can be gauged by comparing the indicial normal-force response of the isolated tail to that of the tail operating in the presence of the wing. This is shown in Figs. 6 and 7 for the panel method and the Euler method, respectively. Examining the potential-flow results, shows that the presence of the wing significantly modifies the tail's aerodynamic response. Unlike the isolated tail's monotonic approach to the final value of the normal force, the tail operating with the wing first experiences an increase, then a decrease on its way to the final value (lower than in the isolated tail case because of the down-wash of the wing). This behavior is brought about by the aft-convecting vorticity, generated at the trailing edge of the wing, and in the panel method represented by a time-variant doublet distribution ($\vec{\gamma}(s_1,s_2,t) = \vec{n}_w(s_1,s_2) \times \vec{\nabla}\mu(s_1,s_2,t)$). The (surface) vorticity due to the change in α on the wake reference surface induces an upwash while it is ahead of the tail and a downwash once it is downstream of the tail.
The maximum of the circulatory part of the response occurs approximately at the average convection time from the wing trailing edge to the tail quarter-chord station. As time increases, the difference between the response of the isolated tail and that of the wing-tail tends towards the steady-flow difference in normal force coefficient.
In contrast to the potential-flow results, the results of the Euler method, see Fig. 7, show the initial response of the tail operating with the wing very similar to that of the isolated tail. This is the result of the finite acoustic-wave convection times represented in the Euler solution. For the condition considered, an acoustic wave travelling with the free stream convects from the wing-root trailing edge to the tail in the time required for the configuration to travel about one half chord. After this time, the vorticity convecting from the wing trailing edge starts to significantly influence the tail's response. Unlike the gradually changing response observed in the potential-flow results, the results of the Euler method show a sudden rise in the nor-

mal force coefficient, followed by a relatively gradual decrease. This may be accounted for in terms of a Doppler effect, as the acoustic waves will tend to coalesce as the vorticity convects towards the tail, and separate as it proceeds aft.

Complete Configuration

As a complete aircraft configuration, the Cessna Citation II flight-test aircraft operated by Delft University of Technology and National Aerospace Laboratory NLR of the Netherlands has been chosen. The geometry considered includes the wing, the tail surfaces, the fuselage, the aft-mounted engine nacelle, the engine pylon and the engine exhaust.

The effects of aerodynamic interactions on the indicial response become more intricate when all components of the configuration are present. For the aircraft configuration considered, the aerodynamics at the tail can be significantly influenced by the presence of the fuselage, engine pylon, nacelle and exhaust stream. These components must be included in the computations in order to obtain accurate induced responses.

The half-domain panel model used as the discretized surface of the configuration is shown in Fig. 8. The number and position of the various components of the configuration makes the specification of properly chosen wake reference surfaces more challenging than in the previous two cases. An example is the wake from the pylon, which must remain first attached to the fuselage and then to the plane of symmetry of the configuration in order to maintain a correct panel model. An incorrectly positioned or distorted wake reference surface can result in high local loads on the fuselage, or reduce the stability of the Newton-Raphson iterative procedure for the relaxation of the doublet distribution on the wake reference surface. As the number of aerodynamic components present in this region makes a priori estimates of the local flow difficult, some trial and error was required to establish an acceptable panel model. For the potential-flow computations a total of 3162 panels were used. The engine intake was represented by a disk at the fan face within the engine nacelle, with a normal flow specified corresponding to the engine setting. The engine exhaust stream was modelled as a solid body continuing several fuselage lengths downstream from the nacelle trailing edge.

For the application of the Euler method a carefully tuned grid with 1.7 million cells in the half-space was generated, see Fig. 9. The grid employs an overall CH-topology, with embedded C-grids for the wing, tail, nacelle, pylon and fin. The embedded C-grids were used to avoid the skewed leading-edge cells produced by simple H-topologies, which tend to adversely affect the solution quality. In order to capture the initial (non-circulatory) pressure perturbation transients, excessive stretching of the surface grid away from the leading and trailing edges was also avoided. The provision of an adequate grid resolution in the wing-wake region was complicated by the lay-out of the aircraft. The grid topology employed allows the main wing trailing-edge block line to sweep upwards with the lower surface of the fuselage as it proceeds aft. This tends to pull the regions with high levels of discretization near the wing trailing edge away from the region through which the wing vorticity will pass. The addition of high curvature to the block interface or the introduction of additional blocks were found to be undesirable alternatives, as they considerably increase cell skewness. Thus a finer discretization below the wing was required to maintain adequate wake resolution in the aft part of the computational domain.

The engine exhaust stream was included in the simulation in order to provide an accurate representation of the flow near the tail. The most efficient grid topology for the exhaust duct was found to be non-annular, complicating the application of the hot and cold exhaust boundary conditions. To avoid the loss of efficiency incurred with excessive sub-division of the domain, the hot and cold exhaust flows were specified using a patched boundary condition. In this procedure the faces of the cells overlapping the divisions between the different exhaust streams were sub-divided into triangles, each of which belong fully to either the hot or the cold stream.

The indicial plunge response was excited by imposing a step change in angle of attack of 2.5 deg on an initial steady-flow solution for $\alpha = 0$, brought about by a discontinuous change in the grid velocity. The Mach number for the numerical simulation with the Euler method is 0.5.

The very rapid nature of the transients during the initial, mainly non-circulatory, portion of the response is illustrated in Figs. 10 and 11 which show at two points in time the incremental pressure distribution on the configuration and the incremental downwash in the wake. At $t = 0.001$s the change to the steady-flow pressure distribution shows regions of uniform perturbation, corresponding to the result of the piston theory, and the start of the creation of compression and expansion waves from the edges. The vorticity generated by the wing is visible as a rapid change in the vertical velocity distribution just aft of the trailing edge. At $t = 0.01$s, the initially uniform pressure perturbation has already evolved towards its final steady-flow distribution. The effect of the vorticity generated by the wing is now visible as a band just over one tip chord downstream of the trailing edge. At still later times, the downstream convection of the vorticity, and its effect on the flow around the tail surfaces, plays a major role in determining the asymptotic form of the indicial response.

Fig. 12 shows for the wing-tail configuration the pattern of isolines of the downwash in a vertical plane, downstream of the wing trailing edge but ahead of the tail, as

obtained from the Euler solution. At the time the pattern is shown the vorticity shed by the wing has just passed the plane considered. The plot shows the presence of the tip vortex (region with tightly closed contours), as well as the presence of the wing vortex wake (region where the contours change direction rapidly). Fig. 13 shows the pattern obtained for the complete configuration. Away from the fuselage and engine nacelle the pattern is similar to that for the wing-tail configuration. However, in the region around the nacelle-pylon the downwash field is much more complex, also due to the presence of the fuselage. Since the flow in this region dominates the response of the tail, the inclusion of the nacelle, pylon and fuselage is needed in order to get the correct prediction of the response for the complete aircraft.

Fig. 14 shows the response in the normal-force coefficient of the tail surface in the presence of the complete aircraft. Compared are the result of the potential-flow method and that of the Euler method. The comparison is similar to the one for the wing-tail configuration, see Fig. 3, with the potential-flow result having the initial non-circulatory part reduced to a delta function type pulse, while for the Euler solution the non-circulatory part of the response has a finite duration. For later times the two results approach each other asymptotically, with a small difference in the then remaining circulatory part due to difference in free stream Mach number.

For the potential-flow method Fig. 15 compares the contribution of the tail to the change in the pitching-moment coefficient computed for the tail in isolation, the tail in the presence of the wing and the tail in the presence of the complete configuration. It is clear that the presence of the nacelle, pylon and engine exhaust does attenuate the response of the tail to the indicial excitation. Fig. 16 gives the similar result obtained from the Euler solution, from which the same conclusion can be drawn as far as the circulatory part of the response is concerned. For the non-circulatory part the differences between the various configurations are different, primarily because this part of the response is dominated by the acoustic waves generated on the upper and lower surface of the tail itself.

To give an impression of the computer resources needed for the Euler method: for the numerical simulation of the indicial response to a step change in incidence on a steady-state solution, on the grid with 1.7 million grid points, requires of the order of 45 CPU hours on a single Cray C98 processor. The panel method requires at least one order of magnitude less CPU time, working on a R10000-processor workstation.

Concluding remarks

Dynamic parameters for a complete aircraft configuration have been made employing both a potential-flow method for incompressible flow and an Euler method for compressible flow. The flow features responsible for the specific behavior of these parameters in portions of the indicial response have been identified by comparing results for simpler configurations such as the isolated wing and wing-tail configurations with the results for the complete configuration. Also the effects of compressibility (Mach number) on the response have been linked to the non-circulatory part of the response, where significant differences between the Euler method and the panel method are found. In general the circulatory part of the response as obtained from the two computational methods agree satisfactorily. The presence of the nacelle/pylon/exhaust, and to a lesser extent the fuselage, has a significant effect on the aerodynamic response of the tail, i.e. the response is attenuated. Though the Euler method is better equiped to simulate the flow features relevant to the aerodynamic response, it does require substantial effort in terms of computer resources and especially manhours to generate a grid on which the vorticity fields survive long enough to accurately simulate the aerodynamic interaction with other components of the configuration and therewith the circulatory part of the response.
The potential-flow method does require less effort, but there is the uncertainty related to the proper choice of the wake reference surfaces as well as the absence of the inadequate representation of the non-circulatory part of the response.

Acknowledgements

This research has been made possible by support from the Stichting Nationale Computerfaciliteiten (NCF) of the Netherlands and Cray Research Inc. The authors wish to thank Pratt and Whitney of Canada Inc. and the Cessna Aircraft Company for their technical assistance.
Most of the work described in this paper was carried out at Delft University of Technology, Department of Aerospace Engineering, Delft, The Netherlands.

References

1. Schiff, L.B., Katz, J. "Application of CFD Techniques towards the Validation of Nonlinear Aerodynamic Models", In: *Unsteady Aerodynamics - Fundamentals and Applications to Aircraft Dynamics*, AGARD CP-386, 1985.
2. Hoeijmakers, H.W.M.: "Panel Methods in Aerodynamic Analysis and Design", Chapter 5 in: *Engineering Methods in Aerodynamic Analysis and Design of Aircraft*, AGARD Report R-783, 1988.
3.Tobak, M., Schiff, L.B.: "Aerodynamic Mathematical Modelling - Basic Concepts", AGARD LS-114, Paper 1, March 1981.
4. Etkin, B.E.: "Dynamics of Flight, Stability and Control", John Wiley & Sons Inc., 1982.

5. Bisplinghoff, R.L., Ashley, H., Halfman, R.L.: "Aeroelasticity", Addison-Wesley, Cambridge, Mass., 1955.
6. Leishman, J.G.: "Indicial Lift Approximation for Two-Dimensional Subsonic Flow as Obtained from an Oscillatory Measurement", Journal of Aircraft, Vol. 30, No. 3, pp. 340-351, 1993.
7. Lesieutre, D.J., Reisenthel, P.H., Dillenius, M.F.E.: "A Practical Approach for Calculating Aerodynamic Indicial Functions with a Navier-Stokes Solver", AIAA Paper 94-0059, 1994.
8. Lomax, H.: *AGARD Manual on Aeroelasticity*, Part II, Chapter 6: "Introduction to Indicial Aerodynamics", October 1968.
9. Weber, E.A.C.: "Aircraft Manoeuvring Aerodynamics with an Unsteady, Higher-Order Panel Method, Theory and Application", MSc thesis, Department of Aerospace Engineering, Delft University of Technology, Delft, The Netherlands, September 1995. Also Memorandum M-751, Department of Aerospace Engineering, Delft University of Technology, December 1996.
10. Hulshoff, S.J.: "An Euler Solution Algorithm for Steady Helicopter-Rotor Flows", PhD-Thesis, Department of Aerospace Science and Engineering, University of Toronto, 1994.
11. Venkatakrishnan, V., Jameson, A.: "Computation of Unsteady Transonic Flows by the Solution of the Euler Equations", AIAA Journal, Vol. 26, No. 8, 1988.
12. Jameson, A.: "Time Dependent Calculations Using Multi-Grid, with Applications to Unsteady Flows Past Airfoils and Wings", AIAA Paper 91-1596, 1991.
13. Klopfer, G.H., Molvik, G.A.: "Conservative multizonal interface Algorithm for the 3-D Navier-Stokes Equations", AIAA Paper 91-1601, June 1991.
14. Hulshoff, S.J., Hoeijmakers, H.W.M.: Multi-Block, Multi-grid Euler Computations Using Unstructured Patched Interfaces", Paper presented at European Fluid Mechanics Conference, Göttingen, Germany, September 15-18, 1997.
15. Hulshoff, S.J., Hoeijmakers, H.W.M., Mulder, J.A.: Prediction of Aircraft Longitudinal Response Using Time-Accurate Euler Computations", AIAA Paper 96-2485, 1996.
16. Hulshoff, S.J., Hoeijmakers, H.W.M., Mulder, J.A.: Estimation of Aircraft Dynamic Parameters Using Euler Computations and Comparison with Flight-Test Data", AIAA Paper 96-3416, 1996.
17. Hulshoff, S.J., Hoeijmakers, H.W.M.: Euler Computations for the Indicial Plunge Response of a Complete Aircraft", AIAA Paper 97-2134, 1997.
18. Jones, W.P.: "Aerodynamic Forces on Wings in Non-Uniform Motion", R&M No. 2117, British Aeronautical Research Council, August, 1945.
19. Drischler, J.A.: Calculation and Compilation of the Unsteady-Lift Functions for a Rigid Wing Subjected to Sinusoidal Gusts and to Sinusoidal Sinking Oscillations", NACA TN-3748, 1956.
20. Singh, R., Baeder, J.D.: "Direct Calculation of Indicial Lift Responses of Wings using Computational Fluid Dynamics", AIAA Paper 96-2508, 1996.

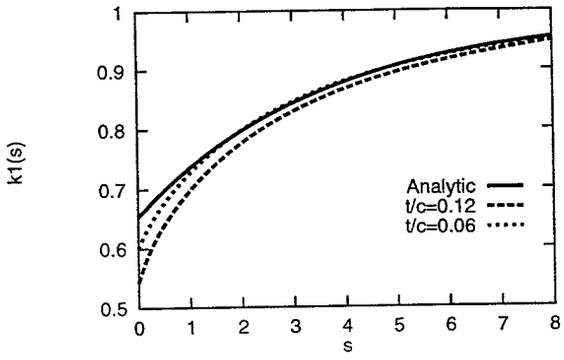

Fig. 1: Finite-span wing of AR = 6, NACA0006 or 0012 airfoil. Indicial lift response computed with panel method compared with analytic solution of Jones[18].

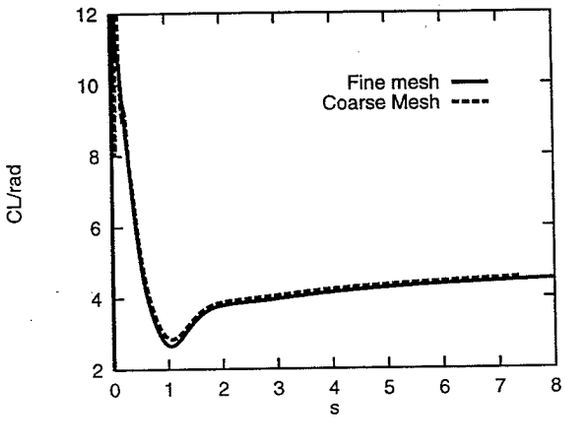

Fig. 2: Finite-span wing of AR = 6, NACA0012 airfoil. Indicial change in lift coefficient per radian computed with Euler method. $M_\infty = 0.3$

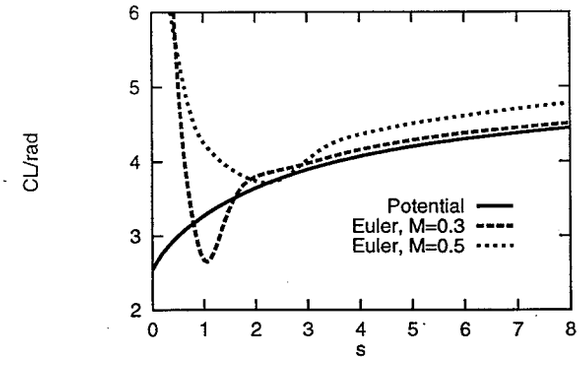

Fig. 3: Finite-span wing of AR = 6, NACA0012 airfoil. Indicial change in lift coefficient per radian computed with panel method (M_∞=0) and with Euler method (M_∞=0.3)

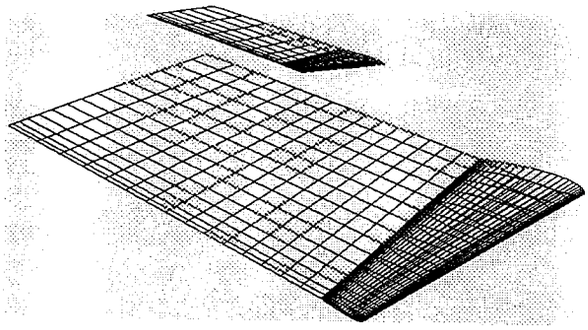

Fig. 4: Wing-tail configuration. Paneling

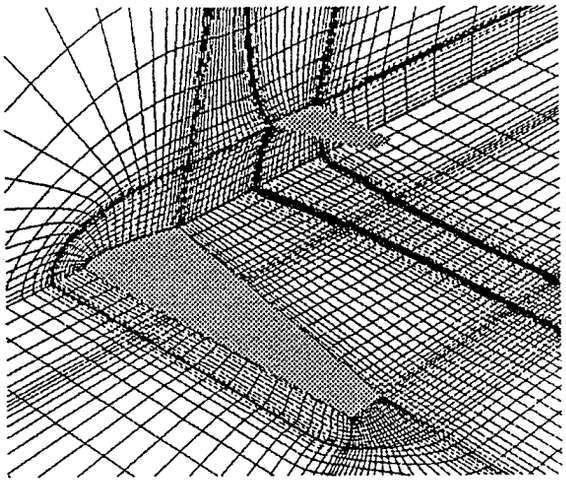

Fig. 5: Wing-tail configuration. Impression of grid
Note: all grid lines are shown

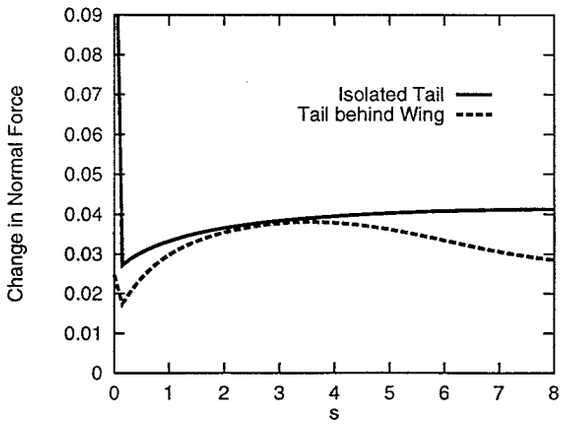

Fig. 6: Indicial change in tail normal-force coefficient of isolated tail and tail in presence of wing, computed with panel method

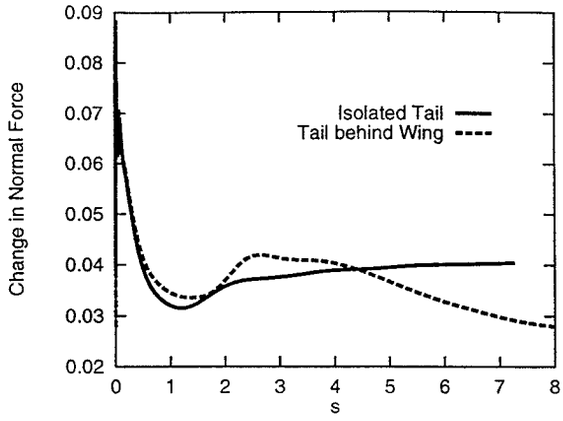

Fig. 7: Wing-tail configuration. Indicial change in tail normal-force coefficient of isolated tail and tail in presence of wing, computed with Euler method ($M_\infty = 0.3$)

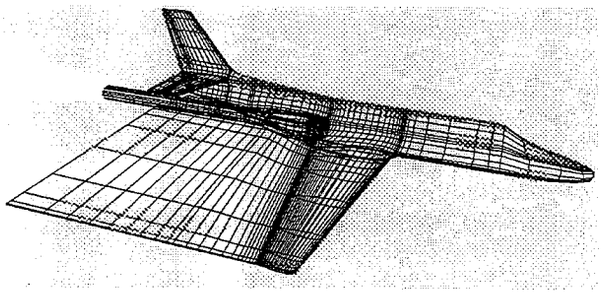

Fig. 8: Complete configuration. Paneling

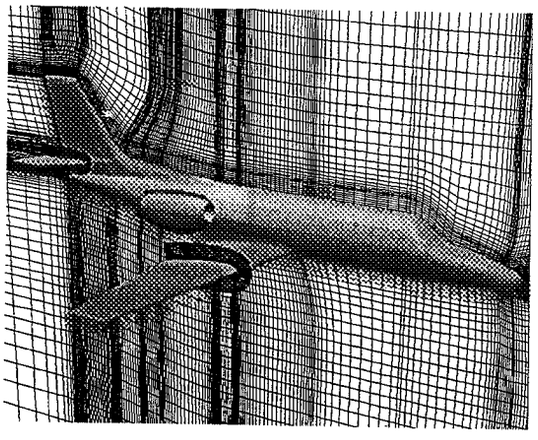

Fig. 9: Complete configuration. Impression of grid

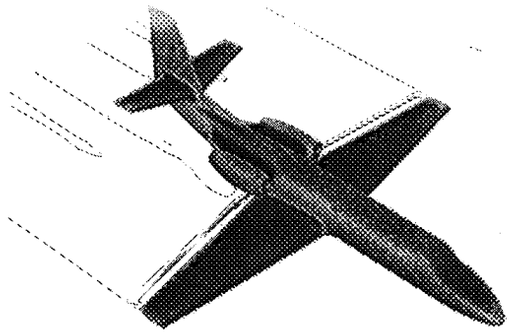

Fig. 10: Complete configuration, $M_\infty = 0.5$. Indicial response computed by Euler method at t = 0.001s. Surface shading indicates change in pressure from the initial steady-flow pressure distribution. Wake refernce plane shows contours of the change in upwash

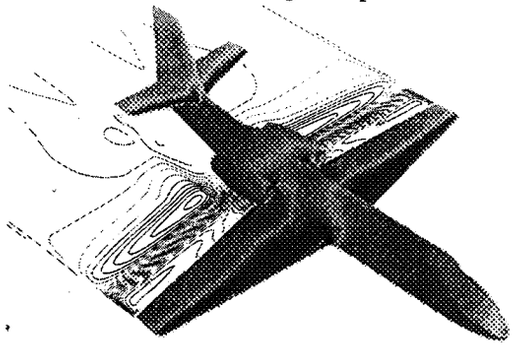

Fig. 11: Complete configuration, $M_\infty = 0.5$. Indicial response computed by Euler method at t = 0.01s

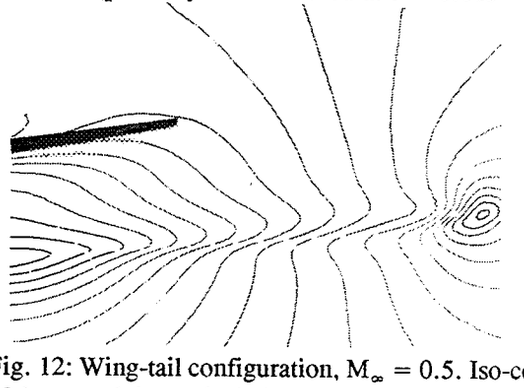

Fig. 12: Wing-tail configuration, $M_\infty = 0.5$. Iso-contours of downwash in vertical plane ahead of tail at time vorticity has convected to tail, computed by Euler method

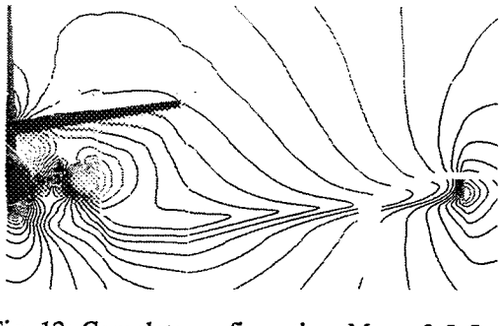

Fig. 13: Complete configuration, $M_\infty = 0.5$. Iso-contours of downwash in vertical plane ahead of tail at time vorticity has convected to tail, computed by Euler method

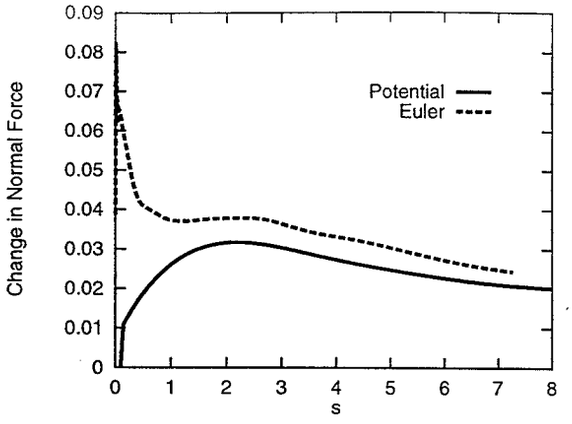

Fig. 14: Complete configuration. Indicial change in tail normal-force coefficient computed with panel method ($M_\infty = 0.0$) and with Euler method ($M_\infty = 0.5$)

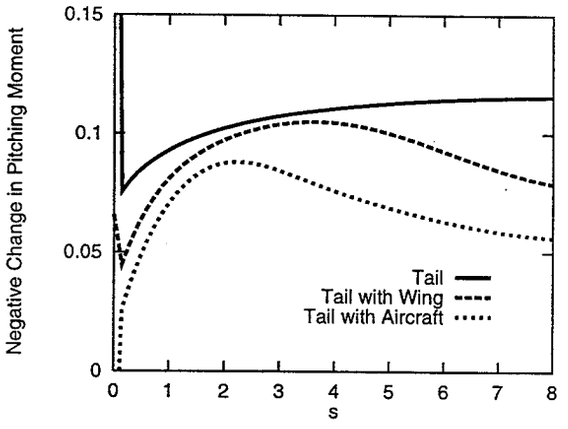

Fig. 15: Complete configuration. Indicial change in tail pitching-moment coefficient of isolated tail, tail in presence of wing and tail in presence of complete configuration, computed with panel method

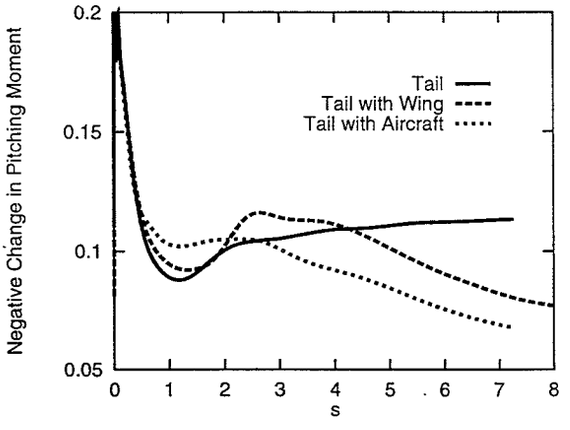

Fig. 16: Complete configuration. Indicial change in tail pitching-moment coefficient of isolated tail, tail in presence of wing and tail in presence of complete configuration, computed with Euler method ($M_\infty = 0.5$)